J|A|C|S
ARTICLES

Published on Web 11/04/2009

Complex Rare-Earth Aluminum Hydrides: Mechanochemical Preparation, Crystal Structure and Potential for Hydrogen Storage

Claudia Weidenthaler,*,† André Pommerin,† Michael Felderhoff,† Wenhao Sun,‡ Christopher Wolverton,‡ Borislav Bogdanović,† and Ferdi Schüth†

Max-Planck-Institut für Kohlenforschung, Kaiser-Wilhelm-Platz 1, 45470 Mülheim, Germany, and Department of Materials Science and Engineering, Northwestern University, Evanston, Illinois 60208

Received June 3, 2009; E-mail: weidenthaler@mpi-muelheim.mpg.de

Abstract: A novel type of complex rare-earth aluminum hydride was prepared by mechanochemical preparation. The crystal structure of the $REAlH_6$ (with RE = La, Ce, Pr, Nd) compounds was calculated by DFT methods and confirmed by preliminary structure refinements. The trigonal crystal structure consists of isolated $[AlH_6]^{3-}$ octahedra bridged via [12] coordinated RE cations. The investigation of the rare-earth aluminum hydrides during thermolysis shows a decrease of thermal stability with increasing atomic number of the RE element. Rare-earth hydrides (REH_x) are formed as primary dehydrogenation products; the final products are RE-aluminum alloys. The calculated decomposition enthalpies of the rare-earth aluminum hydrides are at the lower end for reversible hydrogenation under moderate conditions. Even though these materials may require somewhat higher pressures and/or lower temperatures for rehydrogenation, they are interesting examples of low-temperature metal hydrides for which reversibility might be reached.

Introduction

In the field of hydrogen research, one goal of high priority is the discovery of new hydrogen storage materials for mobile applications, in particular for cars powered by PEM fuel cells.[1] Among the stringent requirements for such materials, most essential are those of high hydrogen storage capacities combined with moderate hydrogen discharge temperatures. At present there is demand for a solid-state hydrogen storage material which allows operation temperatures below 100 °C in a low temperature PEM fuel cell setup. In the past, alkali and alkaline earth aluminum hydrides have intensively been investigated with respect to their potential as solid-state hydrogen storage materials. Unfortunately, the thermodynamic and kinetic properties of most of these compounds are unfavorable for using them in any storage application in low temperature fuel cells under reasonable physical conditions. So far, $NaAlH_4$, doped with transition metals such as Ti, is the only system which works at temperatures around 100 °C.[2] $NaAlH_4$ belongs to the low/middle temperature reversible hydrides with an equilibrium pressure of 0.1 MPa at 30 °C for the first decomposition step and around 100 °C for the second step.[3] The material releases 3.7 wt % hydrogen during the low temperature decomposition step (eq 1). The second decomposition step corresponds to a hydrogen release of 1.9 wt % (eq 2):

$$3NaAlH_4 \rightarrow Na_3AlH_6 + 2Al + 3H_2 \quad (1)$$

$$Na_3AlH_6 \rightarrow 3NaH + Al + 1.5H_2 \quad (2)$$

The rehydrogenation properties of doped $NaAlH_4$ are outstanding compared to other complex aluminum hydrides. Rehydrogenation times of 3−5 min for both steps of a NaH−Al−$ScCl_3$ mixture (molar ratio of 1:1:0.4, 3.5 wt % H_2) have been achieved.[4]

However, certain problems have to be faced with respect to the requirements of low temperature (LT) fuels cells for transportation systems. On the one hand, the decomposition temperature for the second decomposition step is too high to be acceptable for low temperature applications. On the other hand, using only the hydrogen released during the first decomposition step would not be sufficient to run the overall system. In contrast to the intensively investigated light metal aluminum hydrides, at present very little is known about transition metal or rare-earth aluminum hydrides[5,6] and their potential as hydrogen storage materials.[7] While the theoretical hydrogen content of first row transition metal aluminum hydrides is high, they are thermally unstable.[5] Among the rare-earth aluminum hydrides, of particular interest are RE−Al−H systems with RE = La, Ce, Pr, and Nd. Assuming a composition of, e.g., $Nd(AlH_4)_3$, the theoretical hydrogen content for such a

† Max-Planck-Institut für Kohlenforschung.
‡ Northwestern University.

(1) Eberle, U.; Felderhoff, M.; Schüth, F. *Angew. Chem., Int. Ed.* **2009**, *48*, 6608.
(2) Bogdanović, B.; Schwickardi, M. *J. Alloys Compd.* **1997**, *1*, 253.
(3) Bogdanović, B.; Brand, R. A.; Marjanović, A.; Schwickardi, M.; Tölle, J. *J. Alloys Compd.* **2000**, *302*, 36.
(4) Bogdanović, B.; Felderhoff, M.; Pommerin, A.; Schüth, F.; Spielkamp, N.; Stark, A. *J. Alloys Compd.* **2009**, *471*, 383.
(5) Kost, M. E.; Golovanova, A. I. *Izv. Akad. Nauk. SSSR, Neorg. Mater.* **1979**, *14*, 1348.
(6) Barron, A. R.; Wilkinson, G. *Polyhedron* **1986**, *5*, 1897.
(7) Orimo, S.; Nakamori, Y.; Eliseo, J. R.; Züttel, A.; Jensen, C. M. *Chem. Rev.* **2007**, *107*, 4111.

compound is 5.1 wt % which reaches the storage densities required for technical applications, if all other factors would meet requirements as well. Recently, the combination of a high pressure tank and an unstable metal hydride was discussed as a potential storage system for mobile applications.[8] The authors conclude that a solid material with a storage capacity of 4 wt % would bring this combination close to the requirements for mobile applications. Early reports describe $Yb(AlH_4)_2$ to be quite stable.[9] However, surprisingly up to now no experimental data on such complex rare-earth aluminum hydrides are available. This obvious gap in our knowledge on such relatively simple compounds and the potential use of such solids in hydrogen storage was the incentive to prepare complex rare-earth aluminum hydrides, to study their properties, especially their crystal structures and their thermal stabilities, and to evaluate their potential for hydrogen storage.

This paper will focus on the preparation of rare-earth aluminum hydrides, the crystal structure, and their behavior during thermolysis. We have used a combination of experimental methods as well as first-principles density functional calculations to determine the structure and hydrogen storage properties of these materials.

Experimental Section

Synthesis and Purification. Rare-earth complex aluminum hydrides were prepared by the metathesis reaction of the corresponding trichlorides with a 3-fold excess of sodium aluminum hydride, $NaAlH_4$. For this solid-state reaction, the reagents are mixed in a high energy ball mill under slightly increased (1−15 bar) hydrogen pressures. Reaction times are varied between several minutes and 4−10 h to ensure an almost complete reaction. For tracking the reaction progress a commercial mill (Fritsch P7) equipped with a telemetric system to observe the pressure and temperature evolution was used.[10] Due to air and moisture sensitivity of starting materials as well as products, all operations were performed under a protecting argon atmosphere, using a glovebox or Schlenk techniques. Commercial $NaAlH_4$ (Chemetall) was recrystallized by addition of pentane to tetrahydrofuran (THF) solution.[3] Anhydrous $LaCl_3$, $CeCl_3$, $PrCl_3$, and $NdCl_3$ (Aldrich 99.9%) were used without further purification.

Thermal Analysis. The differential scanning calorimetry (DSC) measurements were performed on a Mettler-Toledo DSC 27HP instrument, using a fully automated program for the evaluation of the DSC data. The peak areas of the DSC curves are expressed in milliwatt units. The peak areas were calibrated on the basis of averaged heats of fusion of In and Zn as standards. The measurements were carried out under argon using typically 5−6 mg of sample, heated in an aluminum crucible with a heating rate of 10 K min^{-1}.

Thermolysis. For thermolysis, the samples were weighed into a glass vessel, and the vessel was connected to an automatic gas buret. A thermocouple allowed recording of the sample temperature during the measurement. The glass vessel was inserted in an oven and heated up at 3 K min^{-1}. The different heating rate compared to the DSC measurements was chosen to ascertain thermal equilibrium during the experiment.

X-ray Diffraction. X-ray powder diffraction experiments were performed on a Stoe STADI P transmission diffractometer using Mo $K\alpha_1$ radiation (0.70923 Å). The instrument is equipped with a primary monochromator and a position sensitive detector. To protect the samples from any contact with atmosphere, all samples were prepared in a glovebox into glass capillaries (0.5 mm diameter) which were sealed. The *in situ* X-ray powder diffraction experiments were performed in a Stoe furnace using fused silica capillaries (0.5 mm diameter) as sample holders. During measurements, the samples were kept under a protective gas atmosphere. Data collection was performed under isothermal conditions. The intensities were collected with an image plate system (IP PSD). Crystal structure refinements were performed with the program TOPAS.[11]

Solid-State MAS NMR Investigations. The solid-state ^{27}Al NMR measurements were performed on a Bruker Avance 500WB spectrometer using a standard 4 mm MAS probe (DVT) either with or without magic-angle spinning (MAS). The spectra were measured by applying single (selective) $\pi/4$ pulses or the usual solid-echo sequence ($(\pi/2)_x - \tau - (\pi/2)_y - \tau -$ acquire) with an appropriate phase cycling. For spin−echo measurements under MAS the pulse spacing τ was set to one rotor period. The rf amplitude, measured on an aqueous $AlCl_3$ solution, was 69 kHz and 138 kHz for the single-pulse and spin−echo measurements, respectively. A relaxation delay of 1 s and MAS frequencies between 8 and 14 kHz were applied. The ^{27}Al spectra were referenced to external 1 M aqueous solution of $AlCl_3$.

Density Functional Theory Calculations. Density functional theory (DFT) calculations were performed using the Vienna Ab Initio Simulation Package (VASP).[12] For exchange correlation, the generalized gradient approximation (GGA) of Perdew and Wang was used.[13] Projector augmented wave (PAW) potentials have been applied, and where available (Nd, Pr, Ce), we used potentials for the trivalent element where the f-electrons are treated as core. For La, which does not have a trivalent potential in VASP, calculations with the softer PAW potential in which the f-electrons are treated as valence have been performed. We used the "normal" potentials for Al and H (as opposed to the "hard" potentials) and a plane-wave basis cutoff energy of 325 eV in all calculations. We have previously found that in similar hydride systems the use of these softer potentials with lower energy cutoff yields very similar energetics to calculations with "hard potentials" and higher energy cutoffs. Thus, softer potentials were used for computational efficiency. For all structures, the Brillouin zones were sampled on Monkhorst−Pack *k*-point meshes with at least 128 *k* points per formula unit. Structural degrees of freedom were relaxed until the forces were below 10 meV/Å and stresses were below 1 kbar.

Results and Discussion

Hydrogen Evolution of Rare-Earth Aluminum Hydrides During Synthesis. The metathesis reaction (eq 3a) is a simple and efficient synthesis procedure for the preparation of complex aluminum hydrides.[14] A complete substitution of all three chloride ions of the RE halides would theoretically result in the formation of $RE(AlH_4)_3$ compounds according to eq 3a. During the synthesis, an increase of the pressure inside the milling vial was observed. This suggests the partial decomposition of the reaction products. Hydrogen evolution starts shortly after the beginning of the milling process and ends after about 6 h of milling time (Figure 1). The H_2 released was collected in a gas buret, and from the measured gas volumes, we calculated the amounts of the samples which decompose during preparation. For the La system 51% of the sample decomposed during synthesis. Sample decomposition rates follow for other systems during synthesis: Ce 60%, Pr 56%, and Nd 57%. The

(8) Mori, D.; Hirose, K. *Int. J. Hydrogen Energy* **2009**, *34*, 4569.
(9) Kost, M. E.; Golovanova, A. I. *Izv. Akad. Nauk SSSR* **1978**, *14*, 1732.
(10) Bellosta von Colbe, J. M.; Felderhoff, M.; Bogdanović, B.; Schüth, F. *Chem. Commun.* **2005**, *37*, 4732.
(11) *Bruker AXS, TOPAS V3.0: General Profile and Structure Analysis Software for Powder Diffraction Data, User's Manual*; Bruker AXS:, Karlsruhe, Germany, 2005.
(12) (a) Kresse, G.; Hafner, J. *Phys. Rev.* **1993**, *B 47*, 558. (b) Kresse, G. Ph. D. Thesis, Technische Universität Wien, 1993. (c) Kresse, G.; Furthmüller, J. *Comput. Mater. Sci.* **1996**, *6*, 15. (d) Kresse, G.; Furthmüller, J. *Phys. Rev.* **1996**, *B 54*, 11169.
(13) Perdew, J. P.; Wang, Y. *Phys. Rev.* **1992**, *B 45*, 13244.
(14) Mamatha, M.; Bogdanović, B.; Felderhoff, M.; Pommerin, A.; Schmidt, W.; Schüth, F.; Weidenthaler, C. *J. Alloys Compd.* **2006**, *407*, 78.

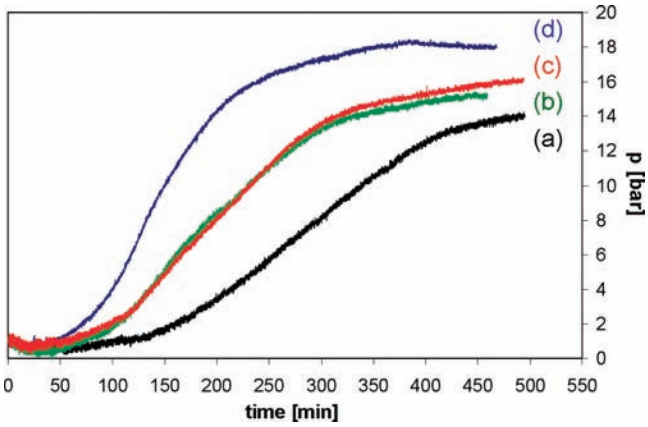

Figure 1. Hydrogen evolution during ball milling of $RECl_3$ with $NaAlH_4$ (1:3), recorded with the help of the telemetry system:[10] (a) La system, (b) Pr system, (c) Ce system, and (d) Nd system.

observation that the samples start to evolve hydrogen during ball milling might be due to the decomposition of a primary, unstable RE aluminum hydride formed during preparation and the subsequent formation of a secondary RE aluminum hydride of unknown stoichiometry (eqs 3a). The evolution of hydrogen is lowest and slowest for the La system and fastest for the Nd system.

$$RECl_3 + 3NaAlH_4 \rightarrow [RE(AlH_4)_3] + 3NaCl \qquad (3a)$$

$$[RE(AlH_4)_3] \rightarrow REAl_xH_y + (3 - x)Al + nH_2 \qquad (3b)$$

At present, the existence of such unstable hydrides which seem to decompose at ambient conditions cannot be proven by additional experimental data. However, the formation of unstable complex aluminum hydrides decomposing under ambient conditions was described for other systems such as $Ti(AlH_4)_4$ and $Fe(AlH_4)_2$.[15,16] Even though the final experimental proof is missing we propose the formation of unstable RE aluminum hydrides with tetrahedrally coordinated Al as working hypothesis.

X-ray Powder Diffraction Experiments. For a qualitative analysis of the ball milling products, all samples were investigated by X-ray powder diffraction methods (Figure 2). Apart from diffraction lines of NaCl and Al, which are formed during the synthesis, additional reflections appear which are marked with an asterisk. These reflections cannot be assigned to any known crystalline phase and are therefore interpreted to belong to a new structure with the theoretical composition $REAl_xH_y$. The similarity of the powder patterns indicates that the crystal structures of the different rare-earth aluminum hydrides have to be very similar. As expected, with increasing atomic number of lanthanide metals $^{57}La \rightarrow {}^{60}Nd$, the diffraction lines shift to higher 2θ values representing decreasing lattice parameters of the new structure with higher atomic number.

Indexing of the Powder Diffraction Pattern of Ce−Aluminum Hydride. Due to the preparation method the products exhibit very small particles which result in broad reflections. These broad reflections make unambiguous indexing very difficult. However, the unit cell seems to have relatively small lattice parameters. Indexing of the powder patterns results in several potential solutions, but only those with the highest figures of merit were considered further. One possible solution is a hexagonal unit cell with $a = 6.47$ Å, $c = 6.26$ Å, and $\gamma = 120°$. The other possible solution is a monoclinic space group with $a = 4.18$ Å, $b = 3.23$ Å, $c = 3.79$ Å, and $\beta = 92.98°$. Indexing was performed with the program DICVOL.[17]

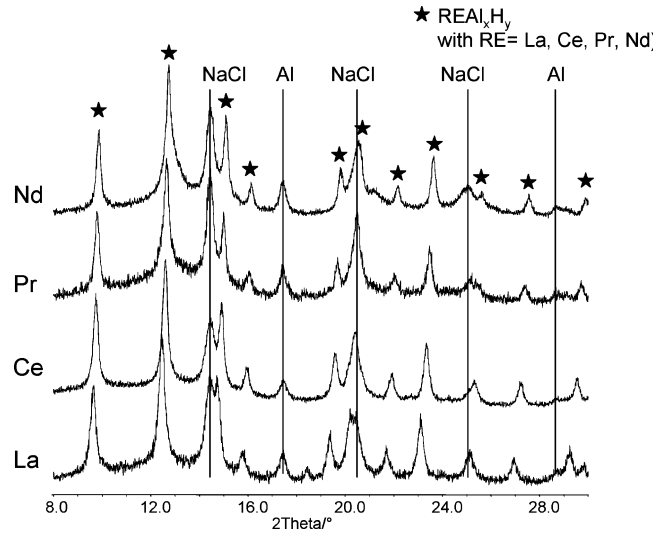

Figure 2. X-ray powder patterns of the different RE−aluminum hydrides collected at room temperature.

Crystal Structure Calculation and First Structure Refinement Results. In an effort to supplement the experimental data and help identify the crystal structure of the $REAl_xH_y$ phase of eq 3b, an extensive series of DFT calculations has been performed. Recently, computational methods have been developed that are capable of the prediction of hydride crystal structures.[18] However, in all of these methods, it is assumed that the stoichiometry of the compound is known. In contrast, in our search for the $REAl_xH_y$ phase, we must first address the unknown stoichiometry of this compound. We hypothesize that the $REAl_xH_y$ compound has a stoichiometry of $REAlH_6$ based on three observations: (1) In other alanate systems, the tetrahydride decomposes initially to form an AlH_6^{3-} anion, and thus, we suspect that one of these anions is a likely candidate for the $REAl_xH_y$ compound. (2) Nd and many other RE elements are known to have stable 3+ oxidation states. Hence, we proceeded with searching for crystal structures with ABC_6 stoichiometry. (3) For the formation of the hexahydride, release of 50% of the hydrogen present in the samples is expected, which is in reasonable agreement with the release experimentally observed (51%, 56%, 57%, and 60%). One of the most popular methods of first-principles crystal structure prediction is to perform "database searching", where one selects candidate crystal structures with similar stoichiometry and reasonable crystal structure types from a database, replacing corresponding atoms with RE, Al, and H, and then finding the structure with the

(15) Kost, M. E.; Golovanova, A. L. *Inorg. Chem.* **1975**, *24*, 905.
(16) Neumaier, H.; Büchel, D.; Ziegelmaier, G. *Z. Anorg. Allg. Chem.* **1966**, *345*, 46.
(17) Boultif, A.; Louer, D. *J. Appl. Crystallogr.* **2004**, *37*, 724.
(18) (a) Wolverton, C.; Ozolins, V. *Phys. Rev.* **2007**, *B75*, 064101. (b) Ozolins, V.; Majzoub, E. H.; Wolverton, C. *Phys. Rev.* **2008**, *L100*, 135501. (c) Ozolins, V.; Majzoub, E. H.; Wolverton, C. *J. Am. Chem. Soc.* **2009**, *131*, 230. (d) Vajeeston, P.; Ravindran, P.; Kjekshus, A.; Fjellvåg, H. *J. Alloys Compd.* **2004**, *363*, L7. (e) Løvvik, O. M.; Swang, O. *Europhys. Lett.* **2004**, *67*, 607. (f) Klaveness, A.; Vajeeston, P.; Ravindran, P.; Fjellvåg, H.; Kjekshus, A. *Phys. Rev.* **2006**, *B73*, 094122. (g) Løvvik, O. M. *Phys. Rev.* **2005**, *B71*, 144111. (h) Mueller, T.; Ceder, G. *Phys. Rev.* **2006**, *B74*, 134104. (i) Voss, J.; Hummelsohj, J. S.; Lodziana, Z.; Vegge, T. *J. Phys. Condens. Mater.* **2009**, *21*, 012203.

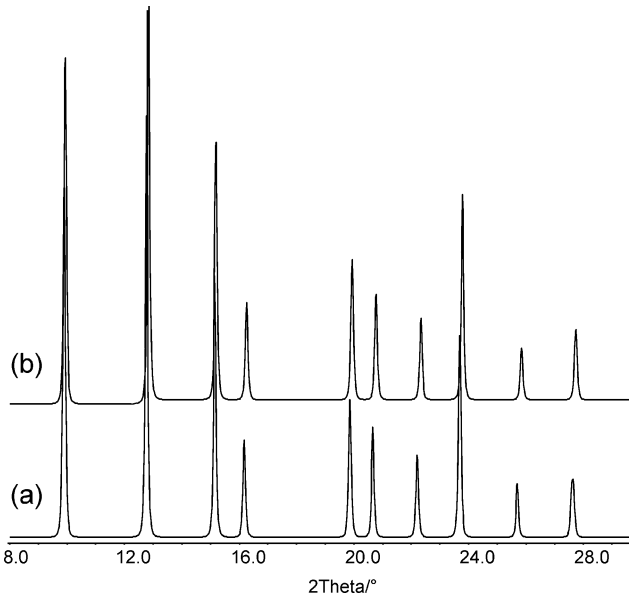

Figure 3. Simulated powder patterns of $NdAlH_6$ for Mo $K\alpha_1$ radiation based on the DFT calculations for (a) $BaSiF_6$ and (b) $KOsF_6$.

lowest total free energy using DFT. For this system, database searching was carried out in the same manner as described before by Wolverton and Ozolins.[18] For our candidate crystal structures, we selected ABC_6 structures from the ICSD, where C = D/H, Cl, F, Br, I, and O. We found over 200 ABC_6 structures in the ICSD, but after eliminating isostructural pairs and structures with fractional occupancies, a set of 54 unique candidate structures was found. We performed DFT calculations of $NdAlH_6$ in all 54 structures, and found two low-energy candidate crystal structures: $KOsF_6$ and $BaSiF_6$, which differ by 1.86 kJ/mol, well within DFT error. The next lowest energy structure is 12 kJ/mol higher than these two structures. The structure of $BaSiF_6$ has space group $R\bar{3}m$ (no. 166), whereas the structure of $KOsF_6$ has space group $R\bar{3}$ (no. 148). The simulated powder patterns for $NdAlH_6$ based on both structure candidates are shown in Figure 3. Since the differences are not significant, we decided to perform the structure refinements starting from the $BaSiF_6$ structure with the higher symmetry. For the other RE compounds ($LaAlH_6$, $CeAlH_6$, and $PrAlH_6$), DFT calculations were performed in only these two structure types. The first-principles calculated crystal structure information for all of the $REAlH_6$ compounds in the $BaSiF_6$ structure is given in Table 1.

Table 1. Crystal Structure Data of the Different $REAlH_6$ Compounds Obtained by DFT Calculations Based on the Minimized $BaSiF_6$ Structure in Space Group $R\bar{3}m$, Refined Lattice Parameters, and Calculated Hydrogen Positions[a]

	lattice parameters from DFT calculations [Å]	lattice parameters from Rietveld refinements [Å]	fractional atomic coordinates for H from DFT calculations (Wykhoff position 18 h)[b]
$LaAlH_6$	$a = 6.4732$	$a = 6.5272(4)$	0.2149, 0.7851, 0.4904
	$c = 6.2765$	$c = 6.3212(7)$	
$CeAlH_6$	$a = 6.4711$	$a = 6.4637(4)$	0.2147, 0.7853, 0.4910
	$c = 6.2527$	$c = 6.2609(7)$	
$PrAlH_6$	$a = 6.4217$	$a = 6.4106(7)$	0.2139, 0.7861, 0.4894
	$c = 6.2028$	$c = 6.2118(11)$	
$NdAlH_6$	$a = 6.3796$	$a = 6.3846(7)$	0.2132, 0.7868, 0.4883
	$c = 6.1616$	$c = 6.1741(10)$	

[a] With RE cations on the crystallographic positions (3b) 0, 0, $^1/_2$, and Al on (3a) 0, 0, 0. [b] Kept fixed during Rietveld refinements.

On the basis of the $BaSiF_6$ structure, the coordinates and lattice parameters obtained from the DFT calculations were used as starting parameters for the crystal structure refinements. In these preliminary refinements, only the heavy elements RE and Al are considered, while the hydrogen positions cannot be refined from X-ray powder data. For precise determination of the hydrogen positions, neutron diffraction data of the deuterated structures are required. The refined lattice parameters of $LaAlH_6$, $CeAlH_6$, $PrAlH_6$, and $NdAlH_6$ are summarized in Table 1, and the preliminary refinement plots of the samples containing $CeAlH_6$ and $LaAlH_6$ are shown in Figure 4a,b. The plots show a good agreement between the observed data and the simulated data based on the results obtained from the DFT calculations.

The quantitative Rietveld refinements reveal that the phase compositions of both samples are very similar with NaCl and Al as main crystalline phases. The amount of $REAlH_6$ was determined to be between 10 and 15 mol %. From the stoichiometry of the overall reaction a molar content of 16.6% $REAlH_6$ would be expected, which is in reasonable agreement with the content determined by Rietveld analysis. These results are also confirmed by the observation that already during ball milling 50−60% of the total hydrogen content is released.

The crystal structures of the new compounds are built up of isolated $[AlH_6]^{3-}$ octahedra which are not directly connected.

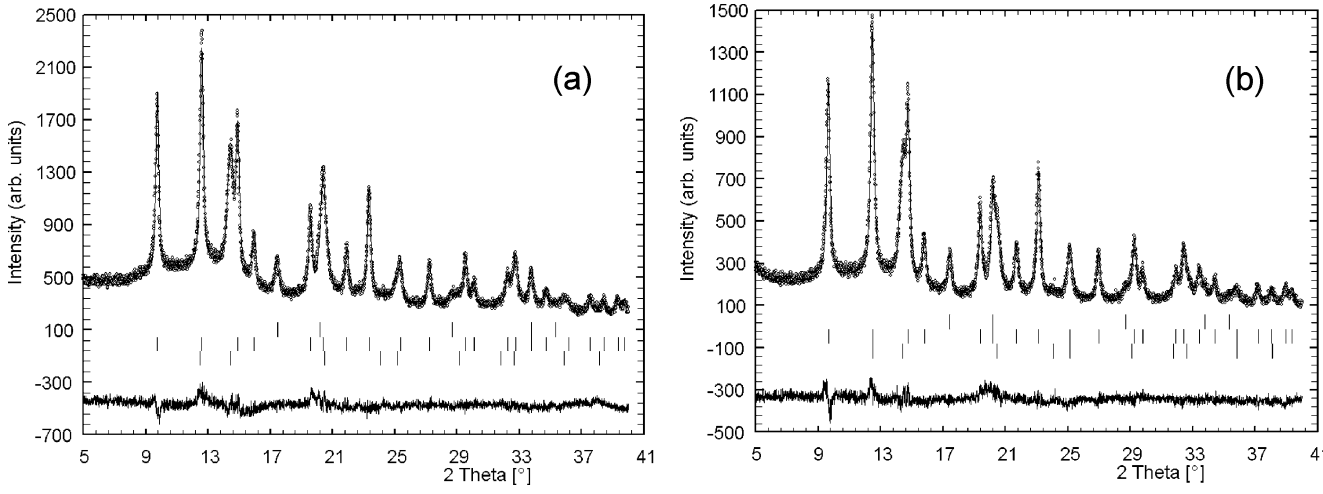

Figure 4. Rietveld refinement plot of (a) the sample containing Al, $CeAlH_6$, and NaCl (the tick marks marking the reflection positions follow this sequence from top to bottom), and (b) the sample containing Al, $LaAlH_6$, and NaCl.

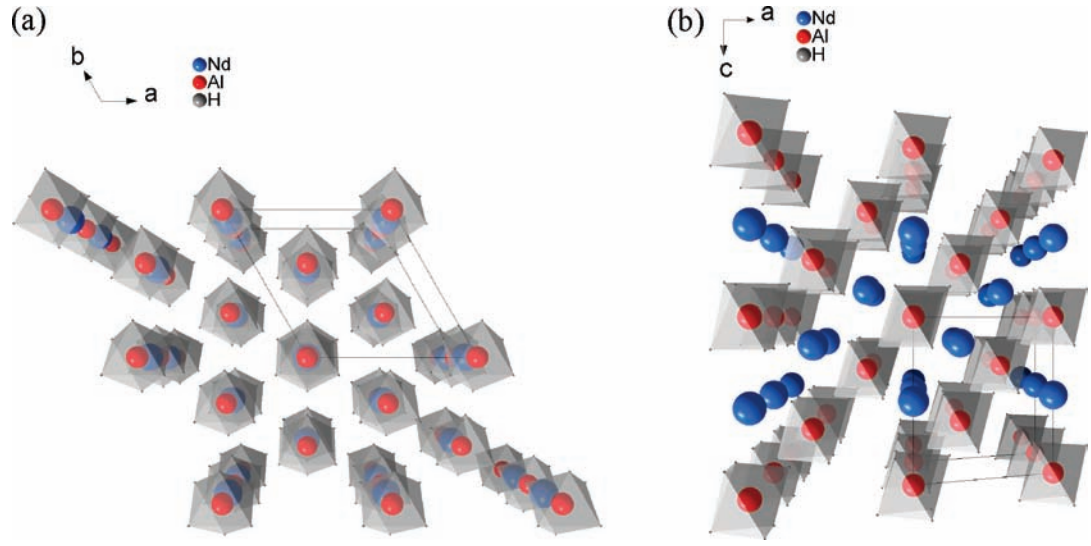

Figure 5. Crystal structure of $NdAlH_6$ in a projection (a) along [001] and (b) along [010].

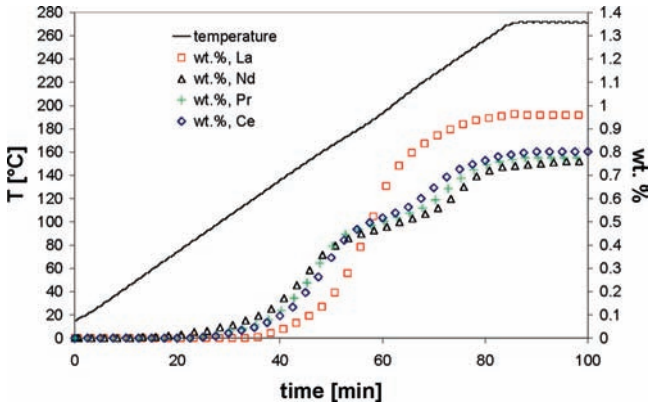

Figure 6. Hydrogen evolution during thermolysis of $LaAlH_6$, $CeAlH_6$, $PrAlH_6$, and $NdAlH_6$ measured up to 270 °C. The amount of hydrogen released has to be related to the overall stoichiometric reaction. All calculations are related to the weight of the entire sample including $REAlH_6$, NaCl, and Al.

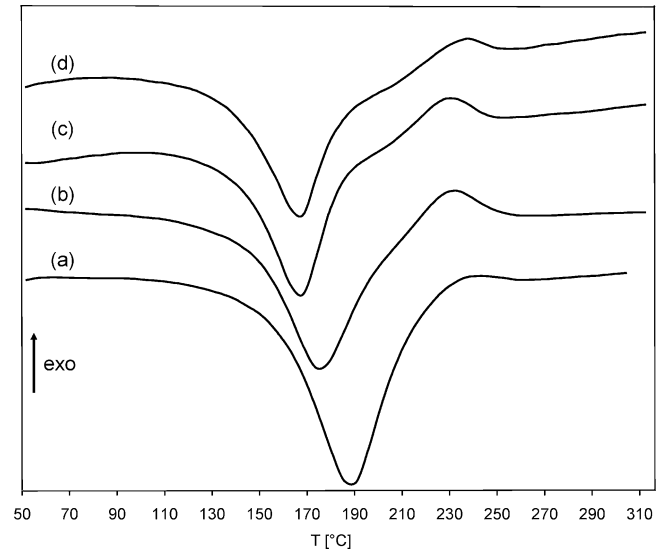

Figure 7. DSC curves of (a) $LaAlH_6$, (b) $CeAlH_6$, (c) $PrAlH_6$, and (d) $NdAlH_6$ recorded with a heating rate of 10 K min^{-1} under protective argon atmosphere.

The presentation of the $NdAlH_6$ structure, which was chosen as a typical example, along the crystallographic *c*-axis shows $[AlH_6]^{3-}$ octahedra alternating with the RE cations forming a chainlike arrangement (Figure 5a).

The view along the crystallographic *b*-axis shows the chainlike arrangement of $[AlH_6]^{3-}$ octahedra between which the RE cations are located (Figure 5b). The coordination of the Nd cations is [12] with 6 coordinating hydrogen atoms in the *ab* plane and 6 hydrogen atoms coordinating the rare-earth cation along the *c*-axis with a slightly larger distance. The precise determination of the hydrogen positions requires the evaluation of neutron diffraction data.

Investigation of Thermolysis by Means of DSC and *in Situ* X-ray Diffraction Experiments. During thermolysis of the different rare-earth aluminum hydrides, hydrogen is released in a two step reaction for Ce, Pr, and Nd whereas only one release step is observed for the La system (Figure 6). For some of the samples, hydrogen evolution starts already at about 100 °C. For Nd, Pr, and Ce significant hydrogen evolution occurs in a first step up to temperatures of about 170−180 °C, and in a second step starting between 170 and 180 °C and finishing between 260 and 270 °C. At higher temperatures no further hydrogen release is observed. For the La sample, hydrogen release starts at higher temperatures, but proceeds much faster, and only one step can be resolved.

The DSC curves of all four samples show a main endothermic reaction with an onset at about 100 °C (Figure 7) followed by an exothermic reaction observable for Ce, Pr, and Nd samples.

Differences of DSC and thermolysis measurements concerning the temperatures of the decomposition steps are an example of how difficult a direct comparison of different analytical tools might be. While the thermolysis curves show two subsequent decomposition steps, the second decomposition is not easy to assign from the DSC curves. Additionally, the second decomposition step appears to happen at higher temperatures. Different heat transfer phenomena, different sample amounts, and different heating rates can be reasons for this observation. However, the two step decomposition is confirmed by *in situ* and *ex situ* diffraction experiments. The main endothermic DSC peak can be related to the decomposition of $REAlH_6$ and the formation of ReH_x. The second step is related to the decomposition of the rare-earth hydride and the formation of an intermetallic com-

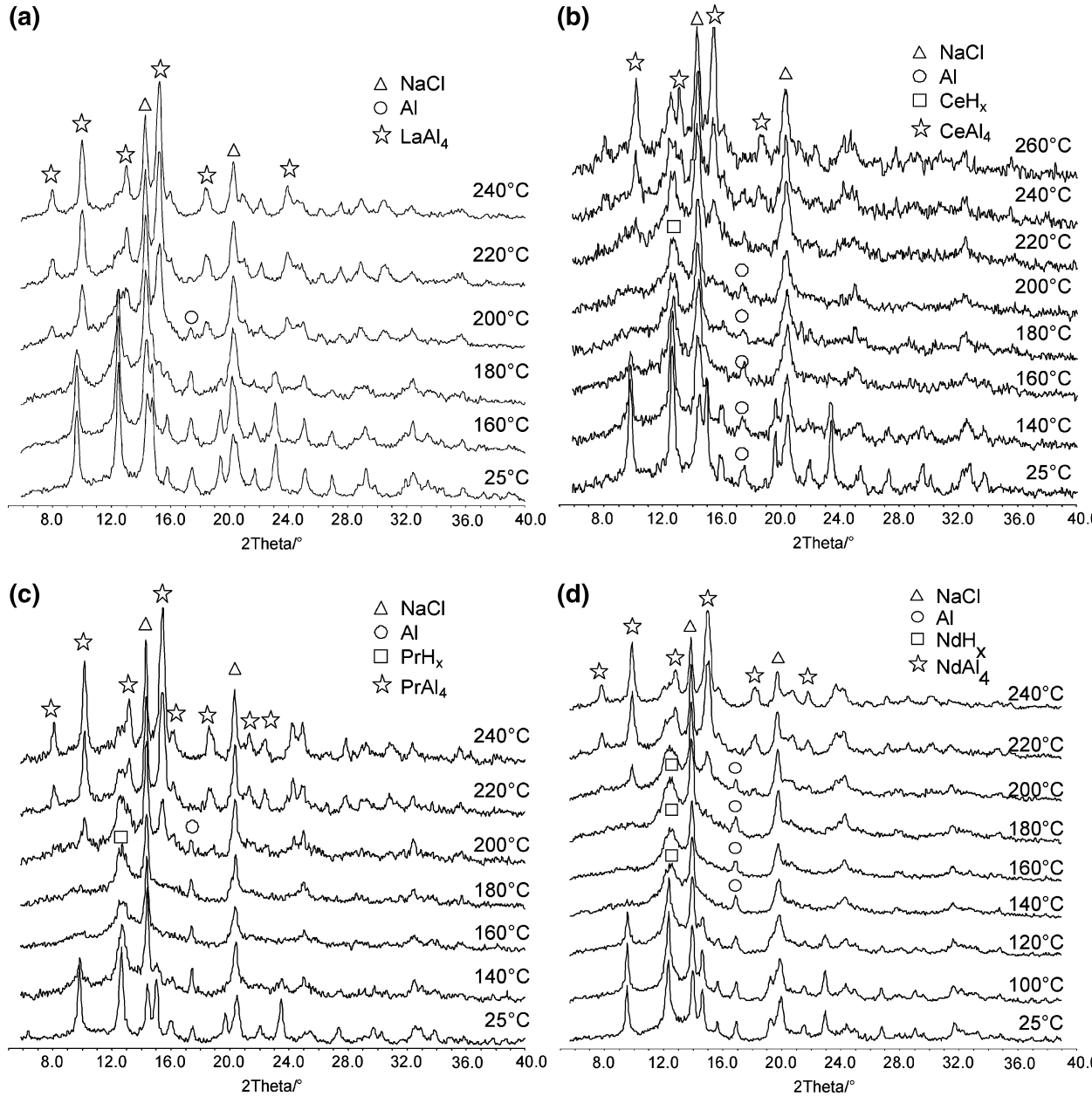

Figure 8. Selection of X-ray powder patterns collected *in situ* during the decomposition (a) $LaAlH_6$, (b) $CeAlH_6$, (c) $PrAlH_6$, and (d) $NdAlH_6$.

pound, $REAl_4$. The decomposition of RE hydrides is an endothermic reaction[19] which proceeds simultaneously with the exothermic formation of the intermetallic compound. Since the energy contribution of the exothermic reaction is larger, the entire process becomes exothermic.

As the *in situ* X-ray diffraction patterns show, the first decomposition step occurs at the highest temperature for $LaAlH_6$ between 180 and 220 °C (Figure 8). The formation of an intermediate LaH_x phase, as observed for the other rare-earth aluminum hydrides, cannot be unambiguously confirmed by the *in situ* XRD data, in agreement with the apparent single step hydrogen release in the thermolysis experiment. However, samples dehydrogenated at defined temperatures and measured after cooling to room temperature show the presence of LaH_x (Figure 9). This suggests that the presence of LaH_x during the *in situ* diffraction experiment is simply missed. Compared to the other rare-earth aluminum hydrides, $LaAlH_6$ is quite stable with a final decomposition temperature of about 200 °C. Already at 200 °C reflections of $LaAl_4$ appear in the powder pattern while no LaH_x is visible. The *in situ* diffraction patterns were collected every 20 °C so that one could easily fail to see the formation of the hydride and observe directly the formation of the intermetallic compound. The decomposition of $CeAlH_6$ starts at slightly lower temperatures and becomes apparent between 140 and 160 °C. The first step of decomposition proceeds via the formation of CeH_x. Above 220 °C CeH_x decomposes and the released Ce and free Al react to form $CeAl_4$. The thermal stability of $PrAlH_6$ is even more reduced, and the decomposition product PrH_x forms already between 130 and 140 °C. However, at 140 °C there are still some reflections of $PrAlH_6$ visible which are completely absent at 160 °C. As already observed for CeH_x, PrH_x is stable up to 210−220 °C before the second step of the

(19) Yartys, V. A.; Gutfleisch, O.; Panasyuk, V. V.; Harris, I. R. *J. Alloys Compd.* **1997**, *253*, 128.

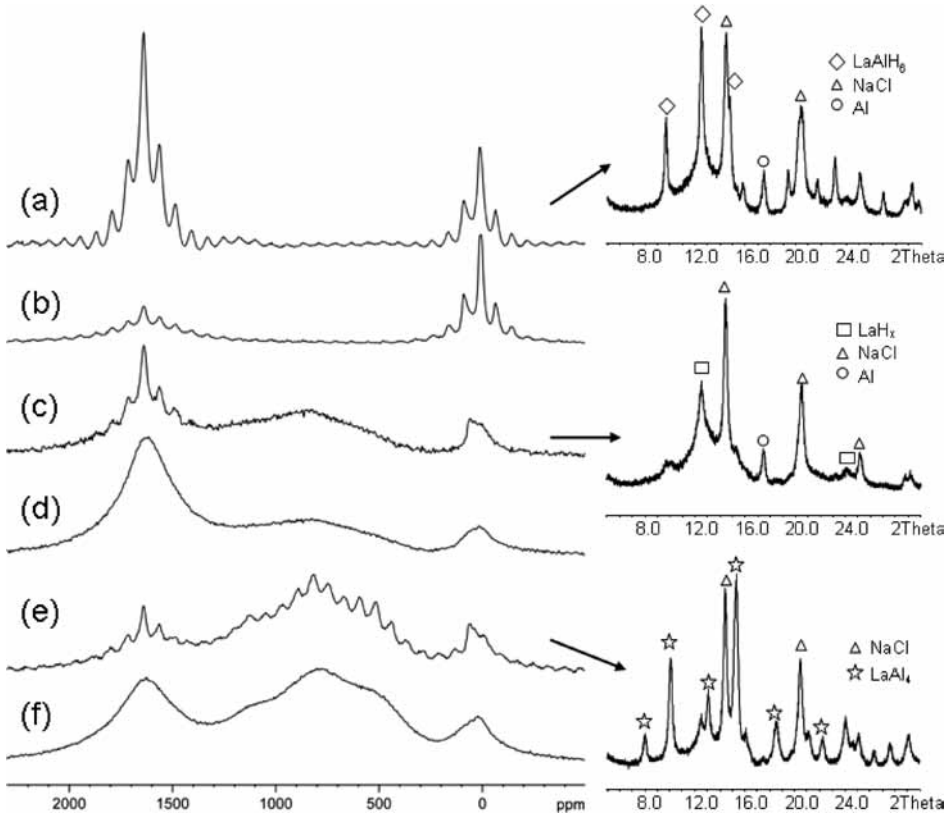

Figure 9. Solid-state ^{27}Al NMR spectra of (a) the $LaAlH_6$-containing sample measured after synthesis at room temperature (Bloch decay, MAS), (b) the MAS spectrum of the sample measured with spin−echo, (c) after heating to 200 °C and cooling to room temperature (spin−echo, MAS), (d) the same sample as in part c but without MAS (spin−echo, stationary sample), (e) sample after heating to 260 °C and cooling to room temperature (spin−echo, MAS), and (f) the same sample as part e but without MAS (spin−echo, stationary sample). For each spectrum, 4000 (a and b) or 32 000 scans (c−f) were accumulated. The MAS frequency was 10 kHz. The XRD patterns show the phase composition after preparation, after partial decomposition at 200 °C, and after decomposition at 260 °C. The data were recorded *ex situ* after cooling to room temperature.

decomposition and the formation of $PrAl_4$ starts. The decomposition of Nd alanate starts at much lower temperatures. The pattern collected at 140 °C does show NdH_x and Al as the only crystalline phases. It is noteworthy that the amount of visible free aluminum does not increase while the aluminum hydride is decomposing. At this point it has to be mentioned that the expected final composition of the intermetallic compound is given by the stoichiometry $REAl_3$. The stoichiometry of the intermetallic compound measured between 240 and 260 °C corresponds to $REAl_4$ which is related to the fact that at these temperatures REH_x is not completely decomposed. Heating the sample to 700 °C (not shown here) leads to a complete decomposition of the hydride and the formation of an alloy of the composition $REAl_3$.

The decomposition enthalpies for the first decomposition step of $CeAlH_6$, $PrAlH_6$, and $NdAlH_6$ (decomposition reaction, e.g., $CeAlH_6 \rightarrow CeH_3 + Al + 1.5\ H_2$) were calculated to be in the range 28−32 kJ/mol H_2. As already mentioned before, the decomposition of $LaAlH_6$ cannot be separated in two distinguishable steps. The decomposition enthalpy of $LaAlH_6$ was therefore calculated for the evolution of all 6 hydrogen atoms, resulting in 30 kJ/mol H_2. For reversible hydrogen uptake at room temperature, the enthalpy should be in the range 30−40 kJ/mol H_2.[20] Thus, the enthalpy values of the rare-earth aluminum hydrides are at the lower end for reversible hydrogenation under moderate conditions, and they will thus probably require somewhat higher pressures for rehydrogenation. Nevertheless, the new aluminum hexahydrides are interesting examples of low-temperature metal hydrides for which reversibility might be reached.

Combining our energies from DFT with the GCLP method of Akbarzadeh et al.,[21] we were further able to compute static $T = 0$ K hydrogen desorption energetics for $NdAlH_6$. For the proposed reaction, we find the results shown in Table 2. The phase included in the GCLP calculations were $NdAlH_6$, H_2, NdH_3, $NdAl_3$, and $NdAl_4$.

A necessary condition for the stability of intermediate phases is that they must lie upon a "convex hull"; that is, stable phases in an endothermic reaction sequence must have increasing molar enthalpies. The energetics obtained from these first-principles calculations confirms the possibility of a two-step decomposition process of the $NdAlH_6$ hydride. Because these enthalpy calculations do not include zero-point energies or finite-temperature contributions, they are only rough approximations. It is generally found that zero-point and $T = 300$ K dynamic corrections can affect $T = 0$ K static enthalpies by as much as 10−20 kJ/mol H_2. Thus, although the static DFT calculated enthalpy for the decomposition of $NdAlH_6$ is lower than the experimental value by 15−20 kJ/mol H_2, this discrepancy could be due to our neglect of vibrational effects in our calculations.

Solid-State ^{27}Al NMR Spectroscopy. Of the lanthanide aluminum hydrides studied, only the lanthanum aluminum

(20) Schüth, F.; Bogdanović, B.; Felderhoff, M. *Chem. Commun* **2004**, 2249.

(21) Akbarzadeh, A.; Ozolins, V.; Wolverton, C. *Adv. Mater.* **2007**, *19*, 3233.

Table 2. First-Principle DFT Static Enthalpies of Decomposition Reactions for the $NdAlH_6$ Hydride[a]

reaction	wt % H_2	ΔH (kJ/mol H_2) static
$NdAlH_6 \rightarrow NdH_3 + Al + \frac{3}{2}H_2$	1.7[b]	13.8
$NdH_3 + 4\,Al \rightarrow Al_4Nd + \frac{3}{2}H_2$	1.2[c]	49.4

[a] These two reactions are predicted by the GCLP method to contribute to the thermodynamically preferred decomposition reaction pathway (see text). Also given are theoretical weight percents for the reaction quoted. These idealized numbers do not account for the weight of the chloride phases or excess Al in the experimental samples. [b] Related to the weight of pure $NdAlH_6$. [c] Related to the weight of $NdH_3 + 4$ Al.

hydride is not paramagnetic. The paramagnetism is caused by the unpaired 4f electrons of all Ln^{3+} ions (except La^{3+} and Lu^{3+}). Hence, we focused our solid-state NMR investigations on the lanthanum aluminum hydride system. The XRD patterns together with the corresponding ^{27}Al NMR spectra of this material at different stages of the decomposition process are given in Figure 9. The X-ray diffraction patterns shown were collected *ex situ* at room temperature, and they represent exactly the samples used for the NMR measurements. The MAS NMR spectrum measured directly after synthesis (Figure 9a) is dominated by the resonance of the metallic aluminum (1640 ppm). This is not surprising since even under ideal conditions $^2/_3$ of the aluminum atoms in the starting mixture would end up in the metallic state. Furthermore, a quantitative interpretation would have to take the effect of the quadrupole interaction into account, whereas for the Al metal, all transitions are observed, and only the central transition might be visible for the other species present. The line at 12 ppm is assigned to lanthanum aluminum hydride. Its position is more than 50 ppm downfield of that of the $[AlH_6]^{3-}$ units in Na_3AlH_6 and about 80 ppm high-field of that of the $[AlH_4]^-$ units in $NaAlH_4$.[22] Nevertheless, we take the observed line position as consistent with the above-described structure. For corner-sharing $[AlH_6]^{3-}$ units in $BaAlH_5$, a structured ^{27}Al NMR line with maxima at about 31 and 20 ppm is observed at the same field.[23] MAS NMR spectra measured at higher spinning rates reveal that there is at least a third line at about 60 ppm (*vide infra*). Apart from the obviously different relative intensities, the spectrum obtained by applying the spin−echo sequence (Figure 9b) gives the same result. The signal of metallic aluminum is strongly reduced. After partial dehydrogenation at 200 °C, the XRD pattern (Figure 9c,d) shows the sample to consist of metallic aluminum, sodium chloride, and LaH_x while the initial $LaAlH_6$ phase has disappeared. In contrast to the *in situ* XRD studies, when the XRD pattern is collected *ex situ*, it was possible to detect LaH_x. As already shown by the DSC measurement and the thermolysis studies, $LaAlH_6$ appears to decompose in a one step reaction at relatively high temperatures of about 180 °C. Concomitantly, LaH_x starts to decompose at about 200 °C simultaneously with the crystallization of the alloy. Therefore, the possibility to miss LaH_x as intermediate phase is relatively high. In the course of the decomposition (Figure 9c) the intensity of the line at 12 ppm decreases and an extremely broad resonance with a maximum at about 830 ppm develops. The position of this line clearly indicates the presence of a Knight shift. Hence, we suggest that it is caused by aluminum atoms in a La_xAl_y phase formed after the decomposition of $LaAlH_6$. Tarasov and co-workers have identified several intermetallic Li_xAl_y phases during the thermal decomposition of $LiAlH_4$.[24,25] As the experimental results (Figures 9c,e) show, the applied spinning rate is far from being sufficient to cause any narrowing of the broad resonance. It just causes some modulation of the line shape for the almost completely decomposed sample. For this sample, the line tentatively assigned to an intermetallic phase is the most intense one which is supported by the XRD data. Since it stretches over more than 250 kHz its shape should be governed by quadrupole interaction and/or Knight shift anisotropy. Obviously, a superposition of several overlapping lines caused by different alloys cannot be ruled out on the basis of our results. The line at about 60 ppm that is clearly visible in the MAS NMR spectra of the decomposed samples is assigned to an oxidic byproduct, most likely produced during the ball-milling.

Conclusion

The successful solid-state synthesis of a new class of rare earth aluminum hydrides by ball milling could be confirmed by several characterization methods. The mechanochemical treatment of rare-earth trichlorides with $NaAlH_4$ or $LiAlH_4$ at room temperature leads to the formation of a compound with the composition $REAlH_6$. A first approximation for the crystal structure was calculated by DFT methods and used as starting point for a Rietveld refinement from X-ray powder diffraction patterns. The structure consists of isolated $[AlH_6]^{3-}$ octahedra connected via rare earth cations. Most alkali and alkaline earth aluminum hydrides which are stable under ambient conditions consist of a structure of $[AlH_4]^-$ tetrahedra as building units. When these initial structures release hydrogen, either hexahydride structures with isolated $[AlH_6]^{3-}$ building units, or structures of connected $[AlH_6]^{3-}$ octahedra,[26] or simple metal hydrides are formed. For the rare-earth aluminum systems no initial structure built of $[AlH_4]^-$ tetrahedra could be observed. However, the fact that significant hydrogen evolution is observed already during the synthesis leads to the hypothesis that at early stages of ball milling a metastable "aluminum tetrahydride" structure might be formed. Such a hypothetical structure is most probably unstable under ambient conditions and decomposes directly to $REAlH_6$. The decomposition of the $REAlH_6$ compounds to REH_x and finally to $REAl_x$ was monitored by *in situ* and *ex situ* X-ray diffraction experiments. The stability of the $REAlH_6$ depends on the atomic number of the rare-earth cation and decreases significantly from La to Nd. The decomposition reaction is endothermic with about 30 kJ mol^{-1} H_2, as revealed by DSC analysis. This suggests that these

(22) Bogdanović, B.; Felderhoff, M.; Germann, M.; Härtl, M.; Pommerin, A.; Schüth, F.; Weidenthaler, C.; Zibrowius, B. *J. Alloys Compd.* **2003**, *350*, 246.
(23) Zibrowius, B. Private communication.
(24) Tarasov, V. P.; Bakum, S.I.; Kuznetsova, S. F. *Russ. J. Inorg. Chem.* **1997**, *42*, 694.
(25) Tarasov, V. P.; Bakum, S. I.; Muravlev, Y. B.; Samoilenko, A. A.; Buslaev, Y. A. *Russ. J. Inorg. Chem.* **1997**, *42*, 1389.
(26) Weidenthaler, C.; Frankcombe, T. J.; Felderhoff, M. *Inorg. Chem.* **2006**, *45*, 3849.

compounds are reversible at lower temperature and/or higher pressure, and thus, these compounds may constitute a new class of intermediate temperature hydrides of which there are not many examples known. Work is in progress in our laboratory to study the effect of catalysts on the dehydrogenation and rehydrogenation behavior.

Acknowledgment. This work was partially supported by General Motors Fuel Cell Activities, in addition to the basic funding by the Max-Planck-Gesellschaft. The work at Northwestern was supported by the U.S. National Science Foundation, under Grant CBET-0730929. B. Zibrowius (MPI) is gratefully acknowledged for solid-state NMR investigation, and U. Holle (MPI) for supporting XRD measurements. The authors would like to thank E. Benser and J. Döring for the preparation of several samples.

JA9042565